Title
Coding of Information in the Phase of Local Field Potentials within Human Medial Temporal Lobe

Journal
Neuron, 79(3)

ISSN
0896-6273

Authors
Lopour, Beth A
Tavassoli, Abtine
Fried, Itzhak
et al.

Publication Date
2013-08-01

DOI
10.1016/j.neuron.2013.06.001

Peer reviewed

Published in final edited form as:
Neuron. 2013 August 7; 79(3): . doi:10.1016/j.neuron.2013.06.001.

Coding of Information in the Phase of Local Field Potentials within Human Medial Temporal Lobe

Beth A. Lopour[1], **Abtine Tavassoli**[1], **Itzhak Fried**[2], and **Dario L. Ringach**[1]

[1]Department of Neurobiology, University of California, Los Angeles, CA

[2]Department of Neurosurgery, University of California, Los Angeles, CA

Summary

There is increasing evidence that the phase of ongoing oscillations plays a role in neural coding, but its relative importance throughout the brain has yet to be understood. We assessed single-trial phase coding in four temporal lobe and four frontal lobe regions of the human brain using local field potentials (LFPs) recorded during a card-matching task. In the temporal lobe, classification of correct/incorrect matches based on LFP phase was significantly better than classification based on amplitude and comparable to the full LFP signal. Surprisingly, in these regions, the correct/incorrect mean phases became aligned to one another before they diverged and coded for trial outcome. Neural responses in the amygdala were consistent with a mechanism of phase resetting, while parahippocampal gyrus activity was indicative of evoked potentials. These findings highlight the importance of phase coding in human MTL and suggest that different brain regions may represent information in diverse ways.

Introduction

Neural coding refers to the representation of external stimuli or behavioral processes in the electrical activity of one or more neurons (Kreiman, 2004). There is increasing evidence that the phase of ongoing neuronal oscillations in sensory areas can code for external stimuli. For example, the phase of an oscillation can outperform the amplitude as a decoder of auditory signals (Ng et al., 2012). Similarly, the addition of phase or phase-of-firing to neural decoding schemes increases the amount of information they provide about a stimulus, as seen in the auditory (Kayser et al., 2009) and visual cortex (Montemurro et al., 2008) of non-human primates. Higher level behavioral processes may also utilize phase coding. In prefrontal cortex, the phase of the gamma oscillation is thought to provide a framework for the encoding of objects in memory (Siegel et al., 2009). Rizzuto et al. (2006) found a similar result in a wide variety of brain regions, reporting that encoding and retrieval of objects in short-term memory occurred at different values of the theta phase. However, a comparison of single-trial coding across multiple brain regions has yet to be completed. In other words, which structures provide information that allows for single-trial classification of neural signals? This is especially interesting in the temporal and frontal lobes where the structures are not necessarily associated with one specific task or sensory modality.

Correspondance: Beth Lopour (bethlopour@ucla.edu).

The mechanism by which phase coding occurs is the subject of much debate (Sauseng et al., 2007). There is evidence from both human EEG (Rousselet et al., 2007) and non-human primate studies (Shah et al., 2004) that the neural response to visual stimuli is the result of a transient evoked potential riding on top of an ongoing oscillation. On the other hand, a *reset* of the phase, with no associated increase in amplitude, has been seen in response to processes of memory (Rizzuto et al., 2003), spatial visual attention (Makeig et al., 2002), and auditory attention (Lakatos et al., 2013). Fell et al. (2004) reported that both evoked potentials and phase resetting contributed to generation of event-related potentials during visual oddball detection and continuous word recognition paradigms. It is unknown how the prevalence of such phenomena varies across brain regions for the same task. Are different regions of the brain associated with different mechanisms? How is each mechanism related to the demands of the task?

Here we study single-trial phase coding simultaneously in eight different regions of the human brain (four in the temporal lobe and four in the frontal lobe) using local field potentials (LFPs) recorded during a card-matching task. We assess the relevance of the localized neural signals to phase coding and test two possible mechanisms associated with the responses in each brain region.

We find that, in discriminating between correct and incorrect trials, the phase of a narrowband LFP signal centered at 2Hz is almost as effective as the full LFP signal and is superior to the amplitude. In addition, the ability to classify single trials is significantly better in regions of the temporal lobe as opposed to the frontal lobe. We also analyze the dynamics of the temporal lobe neural response, finding that the mean phases of correct and incorrect trials become aligned just after the stimulus appears. Lastly, we examine the mechanisms by which these responses are generated. The data from the amygdala are suggestive of phase resetting, while responses in the hippocampus, parahippocampal gyrus, and entorhinal cortex exhibit characteristics consistent with an evoked response. Altogether, these data highlight the prevalence of low-frequency phase coding in the medial temporal lobe (as compared to the frontal lobe) and suggest that individual brain regions may operate differently. In other words, not all brain areas use the same neural code.

Results

Evoked responses differ for correct and incorrect trials and have a strong 2Hz component

Six subjects performed a card-matching task similar to the classic “memory” card game (Fig 1A). Sixteen face-down cards were presented on a laptop computer screen, and the goal was to identify the eight pairs of matching cards by turning over two of them at a time. For each pair chosen by the subject, the two cards either matched (a “correct” response) or did not match (an “incorrect” response). Microwire electrodes were implanted in various brain regions as part of surgical planning for epilepsy, and the local field potential (LFP) was measured during the task. Relative to the onset of the visual stimuli, the average LFP responses for correct and incorrect trials were typically similar after the presentation of the first card, but they differed after the second card was revealed (Fig 1B). The power spectra of the average LFP responses triggered on the opening of the second card showed a dominant component at ~2Hz (Fig 1C). This was consistent with the baseline power spectra (Fig S1A), where many electrodes exhibited power at 2Hz that was above expected levels (Fig S1B). This suggests that the stimulus-locked response may involve the modulation of an ongoing oscillation.

There are different ways in which the modulation of the amplitude and/or phase (Fig 2A) of an ongoing oscillation can shape the average local field potential. This is most readily understood by comparing three idealized, simulated examples. First, if the amplitude is

modulated, but the phase is random from trial to trial, then the result is an *induced oscillation* (Fig 2B, *left*). Second, if there is no change in amplitude, but the phase is adjusted such that it reaches a specific value at a fixed time after the stimulus, a so-called *phase reset* occurs in each trial (Fig 2B, *right*). Third, in the case of an *evoked potential*, a waveform of a given shape is added to an ongoing oscillation of arbitrary phase in each trial, affecting both the phase and amplitude (Fig 2B, *middle*). These three types of responses can occur due to several different physiological phenomena, including dynamic responses to driving inputs and modulatory changes in synaptic connectivity (David et al., 2006).

These examples demonstrate that the phase and amplitude can carry different amounts of information about the behavioral event. It is theoretically possible for the phase alone (Fig 2B, *right*) or amplitude alone (Fig 2B, *left*) to carry all the information, or they can both contribute in part. A central goal of our study is to determine the prevalence of these different response types in the medial temporal and frontal areas of the human brain. We also aim to better understand these electrophysiological signals by asking which component carries the most information about behavioral events.

In the temporal lobe, classification based on ~2Hz phase rivals classification using the full LFP

We used the LFP measurements, triggered on the first and second card presentations, to calculate the discriminability index d' between correct and incorrect trials. This was done using the full LFP signal (d'_{LFP}) and using the amplitude (d'_{amp}) and phase (d'_{phase}) of the signal at a given frequency after decomposing the LFP using a wavelet transform (Fig 2A, see Methods). There was a clear dependence of d' on frequency (Fig 3A). Discriminability was low for phase and amplitude after the first click (Fig 3A, black lines), but it was substantially higher for phase than amplitude after the second click (Fig 3A, red lines). The differences between d'_{amp} and d'_{phase} were greatest for frequencies below 4Hz (Wilcoxon sign-rank test, p=1e-36 at 2.14Hz, see also Fig S2A), and the largest average value for d'_{phase} occurred at 2.14Hz.

Interestingly, in addition to differences between phase and amplitude classifiers, there were differences between brain regions. The values of d'_{phase} in the temporal lobe (n=1008) were significantly larger than those in the frontal lobe (n=644) when measured after the second click (Fig 3B). Again, the largest average d'_{phase} value occurred at a frequency of 2.14Hz, where the difference between temporal and frontal values was greatest (two-sample t-test, p=1e-39, see also Fig S2B).

Looking specifically at 2.14Hz, a scatter plot of all d' values in the temporal lobe confirms that classification using the phase of the LFP is better than classification using the amplitude, and it demonstrates that the d' values based on phase rival those obtained using the full LFP signal (Fig 3C, *top left*). No such relationships were found in the frontal lobe regions, where the d' values were lower (Fig 3C, *bottom*).

To assess the significance of individual d' values, we employed the technique of permutation resampling. For each electrode, all correct and incorrect trials were pooled together. Then two new groups (of equal size to the original correct and incorrect groups) were chosen randomly without replacement, by random assignment of the correct/incorrect labels to each waveform. These two new groups were used to calculate a classifier and an associated d' value. Repeating d' this procedure 1000 times produced a distribution of values under the null hypothesis of independence between correct/incorrect response and waveform shape. If the measured d' value was in the top 5% of this distribution, it was concluded that the result was unlikely to have occurred by chance.

When the analysis was restricted to *significant d'* values based on permutation resampling, classification performance was again superior in the temporal lobe. Out of 1008 bipolar measurements in the temporal lobe, 162 (16.1%) had significant *d'* values. In the frontal lobe, 36 *d'* electrodes out of 644 (5.6%) had significant *d'* values. This trend remained when the data were split into individual brain regions. The amygdala, entorhinal cortex, hippocampus, and parahippocampal gyrus had higher mean *d'* values and a larger percentage of significant values than individual frontal regions (Table 1).

Statistical tests on the significant *d'* values were consistent with the results already presented: following the presentation of the second card, classification based on phase was better than *d'* classification based on amplitude (Fig 4A), and *d'* values in the temporal lobe were higher than *d'* values in the frontal lobe regions (Fig 4B). Therefore, the low-frequency phase in the temporal lobe appears to play a large role in the encoding of stimuli.

Note that the percentage of significant *d'* values in the frontal lobe matches the 5% significance level of the statistical test. It is likely that these are false positives as a result of making multiple comparisons. However, correcting for multiple comparisons in this case is not trivial; the bipolar nature of the electrode measurements means that they are not completely independent from one another, and the fact that all electrodes in a single patient are driven by the same stimulus is another source of correlations between measurements. We therefore choose to focus on the strong results from the temporal lobe and use data from the frontal lobe only as a means of comparison. This highlights the difference between regions where the phase is important for information processing and those where it is not.

In what follows, unless stated otherwise, the analyses will include only those electrodes that were found to have significant *d'* values based on the phase at 2.14Hz, using LFP signals triggered on the presentation of the second image. We will compare the electrodes in the temporal lobe (n=162) to electrodes in the frontal lobe (n=36).

Classification performance in the temporal lobe is associated with a transient increase in IPC

The results presented thus far have shown that, in certain cases, it is possible discriminate between correct and incorrect single trials using the phase of the LFP. This implies that there is a certain amount of consistency in the phase across trials. The intertrial phase coherence (IPC) is a measure of this consistency: at a given point in time, an IPC of zero indicates uniformly distributed phases, and a value of one indicates that all trials have the same phase. In the temporal lobe, there is an increase in IPC that occurs during the presentation of the stimulus for both correct and incorrect trials (Fig 5). The peak values of IPC are reached at 476ms and 591ms for correct and incorrect trials, respectively. In the frontal regions, no increase in IPC is apparent (Fig 5). Therefore, an increase in IPC is one characteristic of LFP signals in the temporal lobe that contributes to classification performance and is clearly different from the behavior of frontal regions.

Dynamics of phase coherence and mean phase difference

The statistical significance of the IPC measurement can be tested by asking the following question: At what point in time during the response are the phases statistically different from a uniform distribution? If the distribution is approximately uniform, the “mean” phase will be the result of noise and will have no meaning. In the temporal lobe, a Rayleigh test of uniformity shows that the phases during both correct and incorrect trials are non-uniform just after the stimulus is presented and remain non-uniform for about 1s (Fig 6A,B, *black lines*). Both mean *p*-values are at or below 0.05 during the time interval t = 119-944ms.

Phases in the frontal lobe electrodes are, on average, uniform over the entire interval and thus do not reach statistical significance (Fig 6A,B, *blue lines*).

Next, given that there is a distribution of phases around each mean, we can ask whether the phase distributions for correct and incorrect responses have different median values. In the temporal lobe, the correct and incorrect trials have statistically different medians (circular Kruskal-Wallis test, $p < 0.05$) during the interval 483-762ms after the onset of the second image (Fig 6C, *black line*). Again, the electrodes in the frontal lobe never reach a level of statistical significance (Fig 6C, *blue line*).

The results of these statistical tests yield some insight into the dynamics of the phase difference between correct and incorrect trials. In the temporal lobe, the mean phase difference across electrodes varies smoothly over time (Fig 6D, *dashed black line*). The phase difference is zero 90ms after the image appears, which roughly corresponds to the beginning of the time interval when the phase distributions are statistically non-uniform (Fig 6D, *dark gray line*). Therefore, there is an alignment of the correct and incorrect phases early in the presentation of the second image. Over time, the phase difference increases, and its peak value at ~π corresponds to the time interval where the median phase values are statistically different (Fig 6D, *green line*). We hypothesize that this similarity in correct and incorrect trials just after the presentation of the stimulus serves as a common starting point for the unique neural responses to the stimulus itself, analogous to the reset of an integrator.

We can verify that the zero mean phase difference is not an artifact of averaging by looking at the fraction of electrodes with a large mean phase difference (Fig 6E). Only 30% of electrodes in the temporal regions have a mean phase difference greater than π/2 when the phase distributions are significantly non-uniform at $t = 119$ms. On the other hand, ~57% of electrodes in the temporal lobe have a large mean phase difference at $t = 500$ms when the IPC values are at their peak. Therefore, the phase difference is likely to be small just after the stimulus appears, and the number of electrodes with large phase differences increases while the image is showing (consistent with Fig 6D). Note that, while the data before t=0 appear smooth and may give an idea of the overall trend, they are not statistically significant.

These analyses highlight the key differences in the phase of LFPs between temporal and frontal regions and provide a clear picture of how the responses develop by first aligning in phase and later developing different means. In addition, the largest phase differences in the temporal lobe coincide with the maximum values of IPC. This is consistent with the idea that a high *d'* value is a product of both an increase in IPC and a large mean phase difference (Rizzuto et al., 2006). More detailed analyses reveal that, as one may expect, d'_{phase} increases with both increased phase coherence and with phase difference between correct and incorrect trials (Fig S3).

Establishing the underlying mechanism: Identification of phase resetting and evoked potentials

The LFP responses observed during the memory task could be generated by different mechanisms. Earlier, we noted that alignment of phases across trials could be caused by a "reset" of ongoing oscillations (Fig 2B, *right*). If this is the case, the oscillation should be present before the stimulus, there should be an increase in phase coherence caused by the stimulus, and there should be no associated increase in amplitude (Shah et al., 2004). Alternatively, the increase in IPC could be caused by the presence of a stimulus-evoked response added to ongoing activity (Fig 2B, *middle*). Such a signal would cause a temporary increase in power at the frequency in question.

In practice, these two mechanisms are difficult to differentiate. Note that the additive evoked response and the phase reset can produce the same average across trials, and the induced oscillation produced no mean response (Fig 2B). Thus, the average signal is not a reliable way to identify the underlying mechanism. Instead, the responses in each electrode can be characterized by the mean amplitude over all trials and the IPC. Note that the amplitude is acquired from the wavelet transform of individual trials of LFP data, so a group of trials can have an increase in mean amplitude, even if mismatched phases cause the mean of the raw LFP signals to be zero. This is the case for the induced oscillation: there is an increase in mean amplitude due to the stimulus, but there is no increase in IPC (Fig 7A, *green*). The evoked potential produces an increase in both mean amplitude and IPC (Fig 7A, *blue*), and the phase reset causes an increase in IPC with no associated increase in mean amplitude (Fig 7A, *red*). Thus, in principle, one can use the relationship between mean amplitude and IPC to identify the mechanism involved.

To assess this strategy, we created idealized models of an induced oscillation, an evoked potential, and a phase reset (Fig 2 and Fig 7A, see also Methods). We then ran 300 simulations of each model. Each simulation represented data from one electrode, and we used different levels of noise for each one. For each electrode, we recorded the IPC and mean amplitude at 600ms after the stimulus. This time was chosen because the peak of the IPC and mean amplitude in the ideal case (no noise) occurred at ~600ms. A plot of the resulting data showed that each mechanism produced a distinct distribution of points in the (IPC, amplitude)-plane (Fig 7B). The induced oscillation was represented by a vertical distribution of points with very low IPC (Fig 7B, *green*), consistent with the amplitude being modulated but phase being random. The evoked potential was associated with a positive correlation between the mean amplitude and IPC (Fig 7B, *blue*). Finally, a phase reset resulted in a distribution where the mean amplitude was essentially flat despite changes in IPC (Fig 7B, *red*).

We performed the same analysis on the LFP data from the card-matching task and grouped the electrodes based on the recording location. Rather than using the amplitude, a *z*-score of the wavelet amplitude was used to account for varying levels of noise and different numbers of trials in each patient. Values of IPC and *z*-score were taken at 534ms, based on an average of the peak IPC times for correct and incorrect trials (Fig 5).

When the data were separated by brain region, they showed evidence for both phase resetting and evoked potentials (Fig 8, Table 1). The amygdala is a candidate for phase resetting, as it has relatively high values of IPC but no statistically significant correlation between IPC and z-score. In stark contrast, the parahippocampal gyrus showed a clear, statistically significant correlation between amplitude and IPC, as one expects in the case of an evoked response. Both the entorhinal cortex and hippocampus also showed statistically significant correlations, but with smaller magnitudes, making a concrete determination of the underlying mechanism a bit more difficult to establish with these data. Similarly, the data from frontal lobe electrodes were inconclusive due to the low values of IPC. Note that by using the correlation coefficient to interpret the data, we are relying on the assumption that all electrodes from a given brain region will behave in a similar fashion. This is a limitation of the present analysis.

Discussion

By using human depth electrode recordings we were able to study the phenomena of phase coding in a variety of temporal and frontal brain regions. The localized nature of these microwire measurements was unique to our study, as previous work in humans was done using electroencephalogy (EEG), electrocorticography (ECoG), or larger intracranial EEG

contacts, often in just one or two regions at a time. First, our results provide evidence that the phase is a key element of information processing in the temporal lobe, where the ability to discriminate between correct and incorrect responses was clearly superior when compared to the frontal lobe (Fig 3 and Fig 4). Second, we report a novel feature of the LFP phase dynamics in response to the stimulus. Surprisingly, we found that the difference between correct and incorrect mean phases is smallest just after the second card is revealed, indicating a process of phase alignment (Fig 6). Later, the mean phases diverge to code for the outcome of the trial. Third, our model-based analysis of the mechanism underlying these responses suggests the presence of an evoked potential in the parahippocampal gyrus and phase resetting in the amygdala (Fig 8).

Coding of behavioral responses using phase

The phase of ongoing oscillations has been found to provide information regarding the coding of individual neural responses during a behavioral task (Kayser et al., 2009; Montemurro et al., 2008; Ng et al., 2012; Siegel et al., 2009). Our data, taken from human depth electrodes, are in agreement with this finding and further suggest that phase coding plays a larger role in the temporal lobe as compared to the frontal lobe. We also find that phase classification is best in the delta band at ~2Hz, consistent with Montemurro et al. (2008); this is a lower frequency than expected, as most studies focus on the theta (4-8Hz) or alpha (8-13Hz) bands.

In an analysis of phase coding, the intertrial phase coherence (IPC) is commonly used to measure the predictability of the phase in response to a behavioral stimulus. It has been found to differ for correct and incorrect responses in a Flanker task (Cavanagh et al., 2009), winning versus losing in a decision-making task (Cohen et al., 2009), remembered versus forgotten words in a short-term memory task (Fell et al., 2008), and relevant/non-relevant stimuli when attending to either visual images or auditory “beeps” (Lakatos et al., 2008). Here we find that, during a card-matching task, there is an increase in IPC only in the temporal lobe. Unlike previous studies, we found that the differences between IPC for correct and incorrect responses were minimal. This confirmed that the IPC alone cannot predict the ability to classify single trials of data. Instead, it is a combination of the IPC and a difference of mean phases, consistent with the findings in Rizzuto et al. (2006).

Phase resetting and evoked potentials

Several recent studies have attempted to distinguish between responses caused by evoked potentials and those due to phase resetting (Sauseng et al., 2007). Fell et al. (2004) used a visual oddball paradigm to compare responses generated by target/non-target stimuli and hits/correct rejections. They found differences in power and “phase-locking” (related to IPC) for each case, specifically with regards to the timing and magnitude. In some cases, they found an increase in phase-locking with no increase in power, suggesting that phase resetting was present. A similar relationship between power and IPC was found in a short-term memory task, again signifying that phase resetting was occurring in response to both list items and the probe (Rizzuto et al., 2003). This reset was often accompanied by a difference in mean phases between the two stimuli, shedding light on potential mechanisms for encoding and retrieval (Rizzuto et al., 2006). Phase resetting has also been seen in response to auditory stimuli (Lakatos et al., 2013; Ng et al., 2012). On the other hand, there have been indications that the event-related potential generated by visual stimuli is due mainly to additive evoked potentials (Rousselet et al., 2007; Shah et al., 2004).

In studying mechanisms of behavioral responses such as phase resetting and additive evoked potentials, a large number of variations are possible (Krieg et al., 2011; Yeung et al., 2007). We have chosen to focus on the simple definition of phase resetting set forth by Shah et al.

(2004): the response is characterized by an increase in coherence with no associated increase in power, and an ongoing oscillation is present before the stimulus. However, while the definition is simple, identification of a mechanism such as phase resetting requires the somewhat arbitrary selection of several criteria. We can measure changes in power using a statistical test, but what significance level is appropriate? Should the change in power be measured relative to baseline values or relative to the pre-stimulus time period? In the case of the IPC, we can again use a statistical test (such as a Rayleigh test of uniformity) to identify time periods of increased phase coherence. However, we must still choose a significance level for the test. For example, an IPC of 0.15 may be statistically higher than chance at some p-value, but visual inspection of the data will give no indication that a phase reset is occurring. Calculating the correlation between IPC and mean amplitude will bypass the need to choose these significance levels, but it may place too high of a value on small deviations from the baseline.

Given that each electrode will have differing amounts of activity across the power spectrum that can obscure the oscillation of interest (here, at 2Hz), we make the assumption that this added noise will lead to smaller changes in amplitude and IPC than we might expect. In other words, an IPC of 0.15 may not be valuable on its own, but its contribution to a larger distribution of points may allow for identification of the underlying mechanism. We therefore introduced a new technique that uses the wavelet amplitude relative to baseline and the IPC, both measured at the peak of the response. Due to the variation in noise across electrodes, it produces a distribution of points for each brain region, and the shape and location of that distribution indicates which mechanism generated the response. This procedure does not require pooling data from electrodes or correct/incorrect responses, and we were able to demonstrate the success of the technique using a mathematical simulation. The data were suggestive of phase resetting in the amygdala and an evoked potential in the parahippocampal gyrus, although the assumption that all electrodes within a brain region will behave similarly may be perceived as a weakness of this analysis.

Phase coding mechanisms may reflect brain region function during the task

By considering the demands of the card-matching task, we can speculate about the relationship between the response mechanism (phase reset or evoked potential) and the brain region in which it occurs. We observe evidence of an evoked potential occurring in the parahippocampal gyrus, a region that is crucial for object-place association in non-human primates (Malkova and Mishkin, 2003). Its specific role appears to be related to the encoding of novel stimuli (Epstein et al., 1999). This is consistent with the observed difference between correct and incorrect trials during the card-matching task; after the second click, if the match is incorrect, a new object-place association must be formed. The images and locations change with each puzzle and are thus a continuous source of novel stimuli. Similarly, the entorhinal cortex is associated with both spatial and object memory (Bellgowan et al., 2009), and the hippocampus is thought to combine information from the “what” and “where” streams (Eichenbaum and Lipton, 2008). Again, consistent with the spatial and object memory requirements of the task, responses in these regions were suggestive of an evoked potential, but they were weaker than those found in the parahippocampal gyrus.

Contrast this with the neural responses in the amygdala, which were more indicative of phase resetting. Properties of this region may explain why this is the case. Phase synchronization between regions of the medial temporal lobe is hypothesized to facilitate communication and aid memory processes (Fell and Axmacher, 2011), and the amygdala is a key component of this (Paré et al., 2002). More specifically, synchrony between the amygdala, hippocampus, and other neocortical regions has been associated with successful recall in an auditory verbal learning test (Babiloni et al., 2009). Therefore, we speculate that

a phase reset in the amygdala may be a mechanism for increasing synchrony and communication with other regions. Note that to increase synchrony between two regions, only one region will need to "reset" to the activity (possibly an evoked response) of the second region.

Relationship between discriminability and underlying mechanism

To the best of our knowledge, the relationship between discriminability (*d'*) and the mechanisms of phase resetting and evoked potentials has yet to be addressed rigorously in the literature. In our study, the three brain regions characterized by correlations between amplitude and IPC also had the largest *d'* values, but there does not appear to be a direct relationship between these features. First, it is important to note that a single *d'* value is calculated based on a comparison of correct and incorrect trials using both training and testing data sets. On the other hand, the IPC and z-score are calculated individually for each data set and response type. This adds to the difficulty of making a direct comparison between these quantities. There are cases where a higher value of the IPC appears to roughly correlate to a higher *d'* value (Fig S4A). Similarly, there are cases where electrodes with a high z-score have high values of *d'* (Fig S4B). There are groups of electrodes in the entorhinal cortex and parahippocampal gyrus that fit both of these criteria, suggesting that higher *d'* values are associated with an evoked potential. However, in viewing the data as a whole, there does not appear to be a clear relationship between *d'* and the mechanism that generated the response. For example, the electrodes in the parahippocampal gyrus with the highest *d'* values do not have the largest values of IPC and have a z-score of approximately zero. This is due to a very small phase difference between correct and incorrect responses (Fig S4C). Therefore, the goal of attributing the phase coding of each brain region to one idealized mechanism is perhaps not as simple as it first appears.

Higher order characteristics of phase

Building on the basic idea of phase modulations in a single electrode, as we have studied here, more complex techniques can be used to demonstrate the importance of phase in neural processes. These techniques involve multiple brain regions and/or data sources. For example, *phase synchrony* (defined as a constant relationship between the phases at more than one electrode) has been hypothesized to facilitate communication between brain regions and play a role in neural plasticity (Fell and Axmacher, 2011; Tiesinga and Sejnowski, 2010). This mechanism has been associated with neural processing for memory (Lega et al., 2012) and attention (Fries et al., 2008). Another phenomenon, *cross-frequency coupling*, occurs when the amplitude of a high-frequency oscillation is modulated by the phase of a lower frequency oscillation (Lakatos et al., 2005; Sauseng and Klimesch, 2008). The phase of the lower frequency is thought to define periods of increased or decreased communication, and this concept has been related to visual processing (Miller et al., 2010), attention (Lakatos et al., 2008), and the response to novel auditory stimuli (Tsunada et al., 2011). Lastly, the combination of single-unit neuronal data with extracellular local field potentials has yielded the notion of *spike-phase coherence*, where the spikes of individual cells fire at a preferred phase of the LFP. It has been shown that spike-phase coherence is correlated with memory strength (Rutishauser et al., 2010) and that the combination of LFP phase and spike timing aids in the decoding of single trial neuronal activity (Kayser et al., 2009).

These concepts could all be applied to the LFP data from the card-matching game, and they therefore present an opportunity for future studies. Inclusion of single-unit data may be a logical first step, as neuronal spikes and LFP are related through synaptic activity. The current study focused solely on the modulation of phase in a single trial at a single electrode,

but an analysis of both spikes and phase across multiple brain regions may shed light on the neural communication involved in these computations.

Experimental Procedures

Participants

We tested six patients (2 males and 4 females, with average age 38.6 +/− 14.0 years) who had been surgically implanted with depth electrodes as part of treatment for medically refractory epilepsy. Each one provided informed consent to participate in the study, which was approved by the Medical Institutional Review Board at the University of California, Los Angeles. The subjects performed the task well, having an average of 87.9 +/− 20.1 incorrect answers for each set of 10 puzzles (80 correct answers). Given the need for the subject to guess the location of the matching cards at the beginning of each puzzle, this baseline level of incorrect answers is expected.

Electrophysiology

The electrode locations were chosen based exclusively on clinical criteria for the purpose of identifying the seizure focus. Typically, the targeted regions included structures in both the temporal lobe (amygdala, hippocampus, entorhinal cortex, parahippocampal gyrus, superior temporal gyrus) and the frontal lobe (orbitofrontal cortex, anterior cingulate gyrus, middle cingulate, supplementary motor area). Each patient underwent whole brain magnetic resonance imaging (MRI) before being bilaterally implanted with 8-12 depth electrodes. After implantation, each patient received a computed tomography (CT) scan which was co-registered to the MRI to verify the placement of the electrodes. The data were initially recorded at 30 kHz using a 128-channel Neuroport system (Blackrock Microsystems, Salt Lake City, UT) and were down-sampled to 2 kHz using the Matlab “resample” function.

In total, we analyzed data from 472 microwires from 59 depth electrodes (Table 1). The depth electrodes had eight 1.5mm wide platinum contacts along the length and eight 40 μm platinum-iridium microwires protruding from the tip. These microwires were used to record extracellular local field potential (LFP) activity. A ninth microwire of lower impedance was available as a reference for the recordings. One of these low-impedance references was used for each group of 32 microwires (4 brain regions). It would have been desirable to use the low-impedance microwire from each depth electrode as a local reference; however, this was not possible due to technical limitations at the time. Because of this, the LFP data was converted to a bipolar montage offline (using software) to ensure that all neural responses were local to the microwire region. The microwires on each depth electrode were not evenly spaced throughout the tissue, so all 28 bipolar combinations were used for each group of 8 microwires. This brings the total data set to (59 depth electrodes)*(28 bipolar combinations) = 1,652 electrode measurements. Note that whenever we refer to data from an “electrode” in the text, we are talking about the bipolar microwire measurements as opposed to the clinical (macro) depth electrodes.

Electrode Referencing

We took special care in choosing a reference montage for our analysis, as it has been shown that using a common reference can sometimes lead to specious results when investigating properties of the phase (Schiff, 2005). The decision to use a bipolar montage was based on the assumptions that (1) the unwanted reference signal was recorded equally by each electrode in the bipolar pair, and (2) each electrode in the pair measured complementary components of the same phenomenon (Zaveri et al., 2006). Assumption (1) is satisfied due to the physical setup of our recording device, and assumption (2) is valid due to the extremely localized measurements of the microwire electrodes. If anything, we would be

concerned that two adjacent microwires were placed so close together that they give exactly the same measurements, and the bipolar pair would thus be useless. The relevant local information would be thrown away with the unwanted reference signal. We can see from the results presented here that this is not always the case, although it may account for the variability of results from each microwire bundle. In general, the use of a bipolar montage is the most conservative choice we can make; it guarantees that the signals used in our analysis are localized to a specific brain region, but it may also reduce the strength the results due to the loss of relevant behavioral information.

Procedure

Patients were presented with a 4×4 grid of face-down cards on a laptop computer screen and were told that there were eight pairs of matching cards (Fig 1A). When they used the mouse to click on a face-down card, the card flipped over and an image appeared. The goal was then to click on the matching card hidden among the other face-down images. After clicking on a pair of cards, matched pairs remained visible, while unmatched images flipped over again after approximately 1 second in order to be matched on a later turn. When all 16 cards were matched, a new puzzle was generated with randomly chosen images and locations. The game contained eight categories of images (e.g. faces, teddy bears, giraffes, watermelons, ice cream, shoes, globes, and waterfalls), with six unique images in each category. Each subject completed 2 sets of 10 puzzles. A set contained 80 correct trials and 87.9 +/ 20.1 incorrect trials, depending on how efficiently the patient completed the task. The experiment was run using the Psychophysics Toolbox in MATLAB.

In our analysis, we draw a distinction between the mouse click on the first image of each pair (“first click”) and the next click on its potential match (“second click”). For the six subjects, the average time between the first and second click ranged from 1.2-2.1 seconds for the first set of 10 puzzles, and it ranged from 1.0-1.7 seconds for the second set of puzzles. The average time between *all* clicks ranged from 1.7-2.3 seconds and 1.5-1.8 seconds for the first and second set of puzzles, respectively. We also divide the trials into two categories: a “correct” trial is one in which the two cards revealed a matching pair, and an “incorrect” trial indicates that the subject chose non-matching cards.

Wavelet analysis of iEEG data

After the recording session, the local field potential data was extracted for each mouse click on a card, which coincided with the presentation of the image stimulus. The segments of data were approximately four seconds long, centered on each click (± 2 seconds). This length was chosen to avoid edge effects in the time range of interest, which was ± 1 second around the stimulus presentation. After resampling at 2 kHz, we removed the mean of each data segment during the presentation of the stimulus. No other filtering was done on the data.

We utilized the free WaveLab toolbox for MATLAB (Donoho, 2005) to perform the wavelet analysis. More specifically, we used the “CWT_Wavelab” function to do a continuous wavelet transform. We chose a complex Morlet wavelet with the following time domain representation:

$$\psi(t) = e^{-\frac{1}{2}t^2}\left(e^{i\omega_0 t} - e^{-\frac{1}{2}{\omega_0}^2}\right).$$

Or equivalently in the Fourier domain,

$$\widehat{\psi}(\omega) = e^{-\frac{1}{2}(\omega-\omega_0)^2} - e^{-\frac{1}{2}\left(\omega^2+\omega_0{}^2\right)},$$

with ω_0 = 5 representing the number of cycles in the wavelet. For the Wavelab function, we chose parameters nvoice = 10, scale = 4, and oct = 6. These settings allowed us to analyze 70 frequencies, ranging from 0.87 Hz to 103.97 Hz (the frequencies varied by 0.1 from −0.2 to 6.7 on a logarithmic scale of base 2). The exact length of each data segment was 8192 data points (4.096 seconds at 2 kHz) to fulfill the requirement of an input signal with dyadic length.

The result of convolving the Morlet wavelet with our LFP data was a complex signal $Z(t)$. We used this to calculate both the instantaneous amplitude

$$A(t) = \sqrt{Re[Z(t)]^2 + Im[Z(t)]^2}$$

and the instantaneous phase

$$\varphi(t) = arctan\left(\frac{Im[Z(t)]}{Re[Z(t)]}\right).$$

These equations are equivalent to the “abs” and “angle” functions in MATLAB. The phase spanned the range [−π, π] with zero being the peak of the oscillation.

As a measure of the baseline activity in each data set, we calculated the average instantaneous amplitude $\overline{A}$ over 1000 randomly selected segments of data. Then, using the standard deviation of amplitude σ_A over the 1000 segments and the number of trials n, we were able to represent the amplitude as a z-score based on the statistics of the population:

$$\tilde{A}(t) = \frac{A(t) - \overline{A}}{\frac{\sigma_A}{\sqrt{n}}}.$$

Single trial classification

The goal of single trial classification is to determine how accurately we can divide single trials of LFP data into two categories based on whether they were triggered on a “correct” response (matching cards) or an “incorrect” response (non-matching cards).

Classification of LFP responses—We begin by using the first data set (10 puzzles with a total of 80 correct trials) to calculate the classifier. Given this limited data set, we chose a linear classifier. For all LFP responses in the data set, we determine the mean of the correct trials $\overline{a}$ and the mean of the incorrect trials $\overline{b}$, and we define the classifier to be $\overline{b} - \overline{a}$. We then project each new single trial p from the second data set onto this classifier by taking the dot product over the time range when the image is visible:

$$q = \int_0^1 p(t)\left(\overline{b}(t) - \overline{a}(t)\right) dt.$$

Here $p(t)$ represents the LFP response from a single trial, with t representing time in seconds. We can calculate the projection q for all correct responses (q_a) and incorrect responses (q_b) from the second data set, resulting in two distributions of this parameter. If the mean LFP responses in these two categories are similar, there will be a large amount of overlap in the distributions. On the other hand, if the responses are distinct, then the distributions will be as well. We measure this with the discriminability index d', which calculates the distance between the means relative to the standard deviation (width) of each distribution:

$$d' = \frac{|\bar{q}_a - \bar{q}_b|}{\sqrt{\frac{1}{2}(\sigma_a^2 + \sigma_b^2)}}.$$

Here $\bar{q}_a$ and σ_a are the mean and standard deviation of q for the correct trials, and $\bar{q}_b$ and σ_b are the mean and standard deviation of q for the incorrect trials. A high value of d' indicates a greater ability to classify correct and incorrect responses on a single trial basis.

Classification using the phase and amplitude of the LFP—The classification based on amplitude is done exactly as described above, with the amplitude substituted for the full LFP signal. Because the phase is a circular quantity, it requires a slight modification of the calculations.

We can represent the phase as a vector quantity in the complex plane,

$$\varphi(t) = \cos\varphi(t) + i\sin\varphi(t) = e^{i\varphi(t)}.$$

Because this is a vector, if we want to sum the phase from multiple trials, we will need to do this separately for the real and imaginary components. Let us define

$$\varphi_x(t) \equiv \sum_{j=1}^{n} \cos\varphi_j(t),$$
$$\varphi_y(t) \equiv \sum_{j=1}^{n} \sin\varphi_j(t),$$

where we are summing over n trials. Then the mean phase over those trials is the angle of the sum of the phase vectors:

$$\overline{\varphi}(t) = \arctan\frac{\varphi_y(t)}{\varphi_x(t)}.$$

We calculate the classifier by determining these sums for the correct and incorrect trials and taking the difference:

$$\Delta_x \equiv \varphi_{x,incorrect} - \varphi_{x,correct}$$
$$\Delta_y \equiv \varphi_{y,incorrect} - \varphi_{y,correct}.$$

And then finally we can project the phase from a new trial θ onto the classifier by taking the dot product in each direction:

$$q=\int_0^1 \cos\theta\,(t)\,\Delta_x\,(t)\,dt+\int_0^1 \sin\theta\,(t)\,\Delta_y\,(t)\,dt.$$

Then, as we did for the full LFP signal, we divide the new trials into correct and incorrect responses, determine the distribution of q in each case, and calculate d'.

Analysis of intertrial phase coherence and mean phase difference

The intertrial phase coherence (IPC) is a measure of the predictability of the phase response across many trials. Mathematically, it is the magnitude of the resultant vector after summing across trials, scaled by the number of trials:

$$C\,(t)=\frac{1}{n}\left|\sum_{j=1}^{n} e^{i\varphi_j(t)}\right|.$$

At time t, if the phase is exactly the same across all trials, the vectors will sum constructively and the IPC will be one. If the phases are uniformly distributed, the vectors will cancel each other, causing the resultant length and IPC to be approximately zero.

For small numbers of trials, a certain level of coherence is expected by chance because it is unlikely that the vectors will have a perfect uniform distribution (Edwards et al., 2009). To account for this, we incorporate a correction based on the number of trials n:

$$IPC^2\,(t)=C^2\,(t)-\frac{1-C^2\,(t)}{n}.$$

Along with the intertrial phase coherence, the mean phase $\bar{\varphi}\,(t)$ can give an indication of the overall response to a stimulus. More specifically, we are interested in the *difference* between the mean phases for different conditions, such as correct and incorrect responses. For two mean phase vectors $\bar{\varphi}_1\,(t)$ and $\bar{\varphi}_2\,(t)$ in the complex plane, we calculate the phase difference $\delta(t)$ using

$$\delta\,(t)=\arctan\frac{|\bar{\varphi}_1\,(t)\times\bar{\varphi}_2\,(t)|}{\bar{\varphi}_1\,(t)\bullet\bar{\varphi}_2\,(t)}.$$

This equation is based on the definition of the dot product $\bar{\varphi}_1\bullet\bar{\varphi}_2=|\bar{\varphi}_1||\bar{\varphi}_2|\cos\delta$ and the magnitude of the cross product $|\bar{\varphi}_1\times\bar{\varphi}_2=|\bar{\varphi}_1||\bar{\varphi}_2|\sin\delta$. In conjunction with the “atan2” function in MATLAB, this will produce a stable measurement of the smaller angle between the two vectors, always in the range $[-\pi, \pi]$.

Mathematical simulations of the underlying mechanism

Simulation of idealized mechanisms—We simulated induced oscillations, additive evoked potentials, and phase resetting at 2Hz with a sampling frequency of 2kHz. Our mathematical models for the three mechanisms were based on the algorithms presented in Krieg et al. (2011). Each trial started with an ongoing oscillation of random phase and an amplitude of one.

We first presented the ideal case for each mechanism with no noise (Fig 2B and Fig 7A) by calculating the mean amplitude and IPC over 1000 trials. The multiplier for the added evoked response (Fig 2B, *middle*) was 1.25 relative to the ongoing oscillation. A wavelet transform was used to calculate the amplitude and phase of each trial; parameters for this were exactly the same as those used for the LFP data.

Simulation of mechanisms with noise—In order to identify the underlying mechanism using the mean amplitude and IPC, we performed the same simulation many times with varying amounts of noise (Fig 7B). All parameters were the same as in the ideal case except the multiplier for the added evoked response was 3. We used 100 trials for each simulation (to approximately match the LFP data), and we performed 300 simulations of each mechanism. Each simulation represented data from one electrode and had additive noise. To create realistic electrophysiological noise, we started with a Gaussian noise signal, took the Fourier transform, and multiplied by a 1/f filter. We then took the inverse Fourier transform and added the real component of the resulting signal to the ongoing oscillation for that trial. The magnitude of the noise increased from 1 to 1500 over the 300 simulations. After generating the noisy trials of data, we used a wavelet transform to determine the amplitude and phase as described above. We then calculated the mean amplitude over trials and the IPC (which was corrected for small n). We recorded each of these values at 600ms, which was the peak of the noise-free response. For the mean amplitude, we subtracted a pre-stimulus baseline measurement, which was the mean amplitude over the time interval t = [−1,0] seconds.

The analysis of the LFP data was performed as described above for the simulated data, except the values of mean amplitude and IPC were recorded at 534ms, and a z-score of the wavelet amplitude $\tilde{A}(t,f)$ was used. Again, a pre-stimulus baseline measurement (the mean of 1s of data before the stimulus) was subtracted from the z-score.

Supplementary Material

Refer to Web version on PubMed Central for supplementary material.

Acknowledgments

Support for B.A.L. was provided by a University of California President's Postdoctoral Fellowship.

References

Babiloni C, Vecchio F, Mirabella G, Buttiglione M, Sebastiano F, Picardi A, Di Gennaro G, Quarato PP, Grammaldo LG, Buffo P, et al. Hippocampal, amygdala, and neocortical synchronization of theta rhythms is related to an immediate recall during rey auditory verbal learning test. Human brain mapping. 2009; 30:2077–2089. [PubMed: 18819109]

Bellgowan PS, Buffalo EA, Bodurka J, Martin A. Lateralized spatial and object memory encoding in entorhinal and perirhinal cortices. Learn Mem. 2009; 16:433–438. [PubMed: 19553381]

Berens P. CircStat: A MATLAB Toolbox for Circular Statistics. Journal of Statistical Software. 2009; 31:1–21.

Cavanagh JF, Cohen MX, Allen JJB. Prelude to and Resolution of an Error: EEG Phase Synchrony Reveals Cognitive Control Dynamics during Action Monitoring. J Neurosci. 2009; 29:98–105. [PubMed: 19129388]

Cohen MX, Elger CE, Fell J. Oscillatory activity and phase-amplitude coupling in the human medial frontal cortex during decision making. J Cogn Neurosci. 2009; 21:390–402. [PubMed: 18510444]

David O, Kilner JM, Friston KJ. Mechanisms of evoked and induced responses in MEG/EEG. Neuroimage. 2006; 31:1580–1591. [PubMed: 16632378]

Donoho, D.; Maleki, A.; Shahram, M. WaveLab. version .8502005.

Edwards E, Soltani M, Kim W, Dalal SS, Nagarajan SS, Berger MS, Knight RT. Comparison of time-frequency responses and the event-related potential to auditory speech stimuli in human cortex. Journal of neurophysiology. 2009; 102:377–386. [PubMed: 19439673]

Eichenbaum H, Lipton PA. Towards a functional organization of the medial temporal lobe memory system: role of the parahippocampal and medial entorhinal cortical areas. Hippocampus. 2008; 18:1314–1324. [PubMed: 19021265]

Epstein R, Harris A, Stanley D, Kanwisher N. The Parahippocampal Place Area: Recognition, Navigation, or Encoding? Neuron. 1999; 23:115–125. [PubMed: 10402198]

Fell J, Axmacher N. The role of phase synchronization in memory processes. Nature reviews Neuroscience. 2011; 12:105–118.

Fell J, Dietl T, Grunwald T, Kurthen M, Klaver P, Trautner P, Schaller C, Elger CE, Fernandez G. Neural bases of cognitive ERPs: more than phase reset. J Cogn Neurosci. 2004; 16:1595–1604. [PubMed: 15601521]

Fell J, Ludowig E, Rosburg T, Axmacher N, Elger CE. Phase-locking within human mediotemporal lobe predicts memory formation. Neuroimage. 2008; 43:410–419. [PubMed: 18703147]

Fries P, Womelsdorf T, Oostenveld R, Desimone R. The effects of visual stimulation and selective visual attention on rhythmic neuronal synchronization in macaque area V4. J Neurosci. 2008; 28:4823–4835. [PubMed: 18448659]

Kayser C, Montemurro MA, Logothetis NK, Panzeri S. Spike-phase coding boosts and stabilizes information carried by spatial and temporal spike patterns. Neuron. 2009; 61:597–608. [PubMed: 19249279]

Kreiman G. Neural coding: computational and biophysical perspectives. Physics of Life Reviews. 2004; 1:71–102.

Krieg J, Trebuchon-Da Fonseca A, Martinez-Montes E, Marquis P, Liegeois-Chauvel C, Benar CG. A comparison of methods for assessing alpha phase resetting in electrophysiology, with application to intracerebral EEG in visual areas. Neuroimage. 2011; 55:67–86. [PubMed: 21111827]

Lakatos P, Karmos G, Mehta AD, Ulbert I, Schroeder CE. Entrainment of neuronal oscillations as a mechanism of attentional selection. Science. 2008; 320:110–113. [PubMed: 18388295]

Lakatos P, Musacchia G, O'Connel MN, Falchier AY, Javitt DC, Schroeder CE. The spectrotemporal filter mechanism of auditory selective attention. Neuron. 2013; 77:750–761. [PubMed: 23439126]

Lakatos P, Shah AS, Knuth KH, Ulbert I, Karmos G, Schroeder CE. An oscillatory hierarchy controlling neuronal excitability and stimulus processing in the auditory cortex. Journal of neurophysiology. 2005; 94:1904–1911. [PubMed: 15901760]

Lega BC, Jacobs J, Kahana M. Human hippocampal theta oscillations and the formation of episodic memories. Hippocampus. 2012; 22:748–761. [PubMed: 21538660]

Makeig S, Westerfield M, Jung TP, Enghoff S, Townsend J, Courchesne E, Sejnowski TJ. Dynamic brain sources of visual evoked responses. Science. 2002; 295:690–694. [PubMed: 11809976]

Malkova L, Mishkin M. One-Trial Memory for Object-Place Associations after Separate Lesions of Hippocampus and Posterior Parahippocampal Region in the Monkey. The Journal of Neuroscience. 2003; 23:1956–1965. [PubMed: 12629201]

Miller KJ, Hermes D, Honey CJ, Sharma M, Rao RP, den Nijs M, Fetz EE, Sejnowski TJ, Hebb AO, Ojemann JG, et al. Dynamic modulation of local population activity by rhythm phase in human occipital cortex during a visual search task. Frontiers in human neuroscience. 2010; 4:197. [PubMed: 21119778]

Montemurro MA, Rasch MJ, Murayama Y, Logothetis NK, Panzeri S. Phase-of-firing coding of natural visual stimuli in primary visual cortex. Current biology : CB. 2008; 18:375–380. [PubMed: 18328702]

Ng BSW, Logothetis NK, Kayser C. EEG Phase Patterns Reflect the Selectivity of Neural Firing. Cerebral Cortex. 2012

Paré D, Collins DR, Pelletier JG. Amygdala oscillations and the consolidation of emotional memories. Trends in cognitive sciences. 2002; 6:306–314. [PubMed: 12110364]

Rizzuto DS, Madsen JR, Bromfield EB, Schulze-Bonhage A, Kahana MJ. Human neocortical oscillations exhibit theta phase differences between encoding and retrieval. Neuroimage. 2006; 31:1352–1358. [PubMed: 16542856]

Rizzuto DS, Madsen JR, Bromfield EB, Schulze-Bonhage A, Seelig D, Aschenbrenner-Scheibe R, Kahana MJ. Reset of human neocortical oscillations during a working memory task. P Natl Acad Sci USA. 2003; 100:7931–7936.

Rousselet GA, Husk JS, Bennett PJ, Sekuler AB. Single-trial EEG dynamics of object and face visual processing. Neuroimage. 2007; 36:843–862. [PubMed: 17475510]

Rutishauser U, Ross IB, Mamelak AN, Schuman EM. Human memory strength is predicted by theta-frequency phase-locking of single neurons. Nature. 2010; 464:903–907. [PubMed: 20336071]

Sauseng P, Klimesch W. What does phase information of oscillatory brain activity tell us about cognitive processes? Neuroscience and biobehavioral reviews. 2008; 32:1001–1013. [PubMed: 18499256]

Sauseng P, Klimesch W, Gruber WR, Hanslmayr S, Freunberger R, Doppelmayr M. Are event-related potential components generated by phase resetting of brain oscillations? A critical discussion. Neuroscience. 2007; 146:1435–1444. [PubMed: 17459593]

Schiff SJ. Dangerous Phase. Neuroinformatics. 2005; 3:315–318. [PubMed: 16284414]

Shah AS, Bressler SL, Knuth KH, Ding M, Mehta AD, Ulbert I, Schroeder CE. Neural dynamics and the fundamental mechanisms of event-related brain potentials. Cereb Cortex. 2004; 14:476–483. [PubMed: 15054063]

Siegel M, Warden MR, Miller EK. Phase-dependent neuronal coding of objects in short-term memory. Proc Natl Acad Sci U S A. 2009; 106:21341–21346. [PubMed: 19926847]

Tiesinga PH, Sejnowski TJ. Mechanisms for Phase Shifting in Cortical Networks and their Role in Communication through Coherence. Frontiers in human neuroscience. 2010; 4:196. [PubMed: 21103013]

Tsunada J, Baker AE, Christison-Lagay KL, Davis SJ, Cohen YE. Modulation of cross-frequency coupling by novel and repeated stimuli in the primate ventrolateral prefrontal cortex. Frontiers in psychology. 2011; 2:217. [PubMed: 21941517]

Yeung N, Bogacz R, Holroyd CB, Nieuwenhuis S, Cohen JD. Theta phase resetting and the error-related negativity. Psychophysiology. 2007; 44:39–49. [PubMed: 17241139]

Zaveri HP, Duckrow RB, Spencer SS. On the use of bipolar montages for time-series analysis of intracranial electroencephalograms. Clinical Neurophysiology. 2006; 117:2102–2108. [PubMed: 16887380]

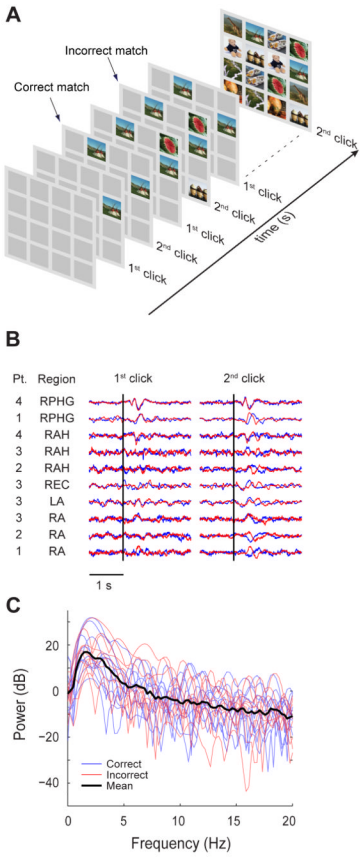

Figure 1.

The card-matching task and mean LFP responses. **(A)** The task was a computer-based card game that required the subject to locate matching pairs of images. Each puzzle contained 8 pairs of images, and each subject completed 2 sets of 10 puzzles. Each "trial" was defined as the opening of a pair of cards anywhere within the puzzle. In a "correct" trial, the two cards matched. Otherwise, the trial was "incorrect." **(B)** The mean LFP responses to correct (blue) and incorrect (red) matches were similar on the first click, but significant differences arose when the subject clicked on the second card. The responses varied over subjects and brain regions (RPHG = right parahippocampal gyrus, RAH = right anterior hippocampus, REC = right entorhinal cortex, LA = left amygdala, and RA = right amygdala). Note that these responses have been scaled to appear the same size; amplitude of the mean LFP varied from 14.81 μV to 367.84 μV. **(C)** The power spectra of the mean LFPs in (B) show a peak at ~2 Hz, indicating that this is the primary frequency contributing to the response. See also Figure S1.

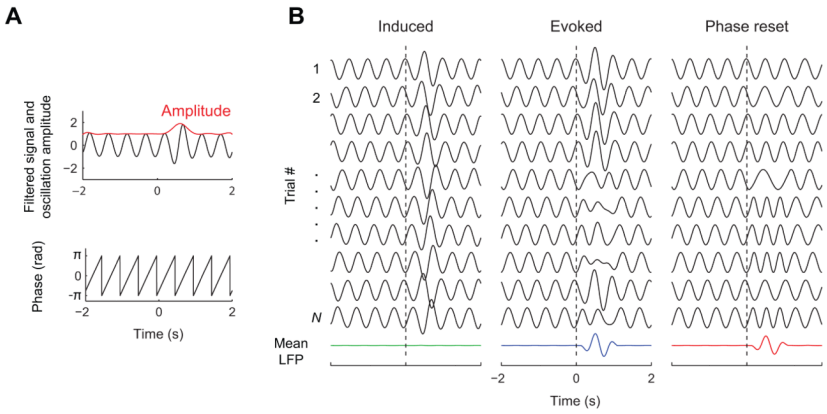

Figure 2.

Different response mechanisms are associated with phase and amplitude carrying different amounts of information. **(A)** Every electrophysiological signal (black line, top), within a narrow frequency band, can be decomposed into amplitude (red line, top) and phase information (bottom). **(B)** LFP responses to a stimulus can be divided into three idealized categories based on the mechanism that generated them: induced oscillations, evoked potentials, and phase resetting. Here, the black traces represent individual simulated trials of LFP, and the colored trace at the bottom represents the mean of 1000 simulated trials. For each trial, the ongoing oscillation has a randomly chosen phase prior to the stimulus. In an induced oscillation (left panel), only the amplitude is altered in response to the stimulus, and the mean across trials is zero (green line). In contrast, a phase reset (right panel) modulates only the phase of the ongoing oscillation, such that it reaches a specific value at a specific time. Here, the oscillation reaches a phase of $\pi/2$ at ~625ms, causing a brief oscillatory mean response (red line). A stimulus-evoked response (middle panel) that is added to the ongoing oscillation will change both the amplitude and phase of the LFP. The mean (blue line) reflects the shape of the evoked potential.

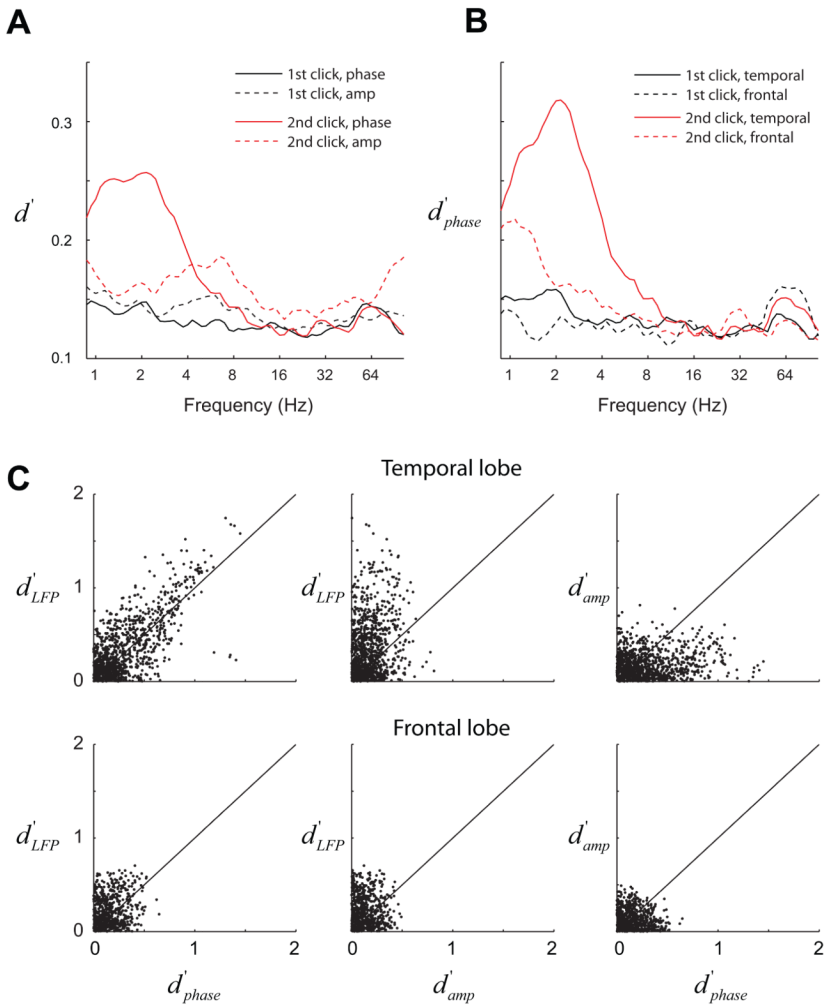

Figure 3.

Comparison of discriminability based on different classifiers (phase, amplitude, raw LFP) and in different brain regions. **(A)** The phase classifier provides better discrimination than the amplitude classifier after the 2nd click, with the largest average value of d'_{phase} occurring at 2.14Hz. This plot shows the mean d' value at each frequency, taken over all 1,652 bipolar electrode measurements. **(B)** The mean values of d'_{phase} in the temporal lobe (n=1008) are superior to those in the frontal lobe (n=644). This panel shows the phase data (solid red and black lines) from (A) after it has been separated by brain region. Again, the peak value occurs after the 2nd click at 2.14Hz. **(C)** In the temporal lobe (top panels), the approximate 1:1 relationship between d'_{phase} at 2.14Hz and d'_{LFP} indicates that they have a similar effectiveness in single-trial classification (top left). Each dot represents LFP data from a single bipolar measurement after the 2nd click. Further, both d'_{LFP} and d'_{phase} at 2.14Hz are superior to discrimination based on the amplitude (d'_{amp}) at the same frequency (top middle and right). Electrodes in the frontal lobe (bottom panels) do not exhibit the same relationships between discrimination based on phase, amplitude, and the full LFP signal. See also Figure S2.

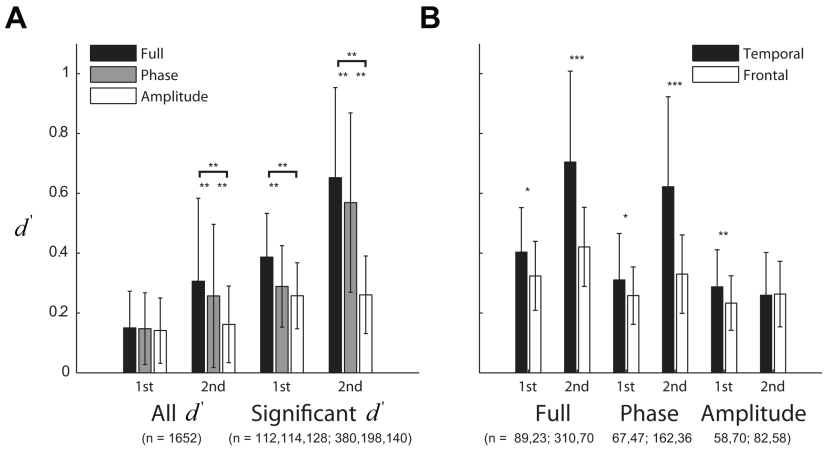

Figure 4.

Statistical analysis of significant *d'* values across classifiers and brain regions. **(A) C**lassification based on phase was better than classification based on amplitude. Here, permutation resampling was used to identify electrodes with significant *d'* values at 2.14Hz. A one-way ANOVA and multiple comparisons test indicate that classifiers based on the full LFP, phase, and amplitude produce significantly different mean *d'* values for the 2nd click. The differences occurred when all *d'* values were included and also when the analysis was restricted to significant *d'* values. All tests were done at a significance of $p = 0.01$. **(B)** Classification in the temporal lobe is superior to the frontal lobe. The differences in *d'* were highly significant for the full LPF classifier and the phase classifier after the 2nd click (two-sample t-test). This panel shows data from significant *d'* values only. In both panels, phase and amplitude were calculated at 2.14Hz, and the vertical error bars indicate standard deviation. Key: * $p < 0.05$, ** $p < 0.01$, *** $p < 0.001$.

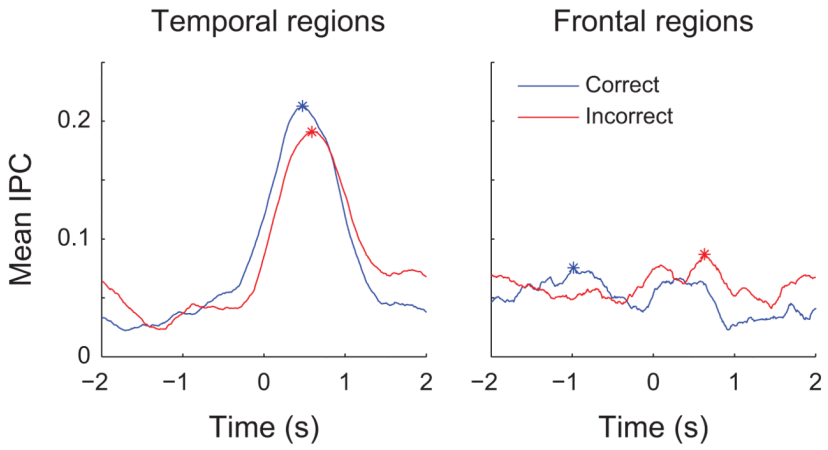

Figure 5.

Phase dynamics in temporal and frontal regions are different. In the temporal lobe (left panel), there is an increase in mean IPC in response to the stimulus for both correct (blue) and incorrect (red) trials. The peak value for correct trials is at 476ms, and the peak value for incorrect trials is reached at 591ms. In contrast, there is no increase in mean IPC in the frontal lobe electrodes (right panel). Both panels show responses following the 2nd click, and the means were calculated using electrodes with significant *d'* values. IPC is based on phase at 2.14Hz.

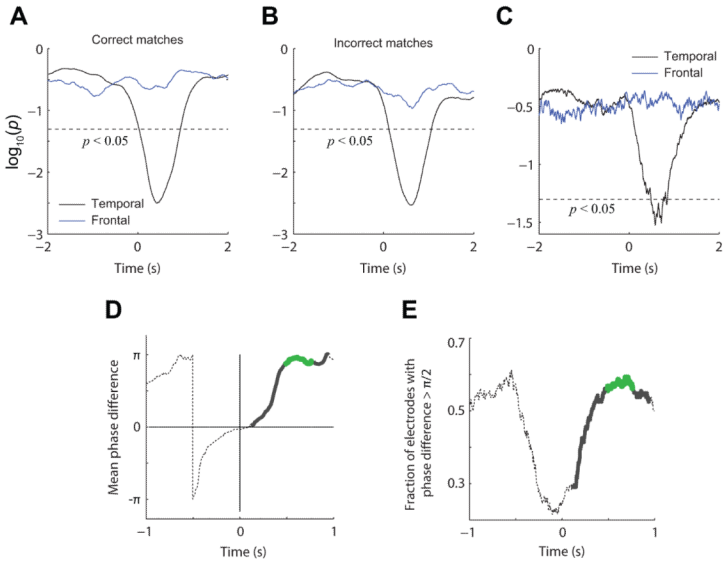

Figure 6.

Dynamics of phase distribution statistics. **(A,B)** In the temporal lobe, a Rayleigh test of uniformity indicates that the phase distributions for both correct (A) and incorrect matches (B) are non-uniform. The mean *p*-values taken over significant electrodes in the temporal lobe (black line) and frontal lobe (blue line) are shown. In the temporal lobe, correct trials meet the criteria $p<0.05$ (dashed line) for 26-944ms after the stimulus, and incorrect trials achieve significance for 119-1063ms after the stimulus. **(C)** For electrodes in the temporal lobe, a test of the median values of the correct and incorrect phase distributions (analogous to the Kruskal-Wallis test) indicates that the median phases are significantly different from one another over the time interval 483-762ms ($p<0.05$, dashed line). Again, this plot shows the mean *p*-value calculated over significant electrodes. Note that the traces were smoothed with a 49-point (25ms) moving average. **(D)** In the temporal lobe, the mean phase difference is small just after the image appears and increases over the course of the trial. For each electrode, we calculated the mean phases for correct and incorrect trials and found the angular difference between the two. We then averaged the phase differences over all significant electrodes in the temporal lobe (dashed line). Time windows of significant non-uniformity (119-944ms, bold gray line) and a significant difference between median phases (483-762ms, bold green line) are shown based on the results from (A-C). **(E)** As a complement to (D), few electrodes have a large phase difference ($>\pi/2$) just after t=0, and this number increases as the image remains visible. This verifies that the results in (D) were not an artifact of averaging a circular quantity. The number of electrodes is shown as a fraction of the total, and statistical significance is marked by bold gray and green lines, as in (D). All circular statistics presented here were done using the free Matlab toolbox CircStat (Berens, 2009). See also Figure S3.

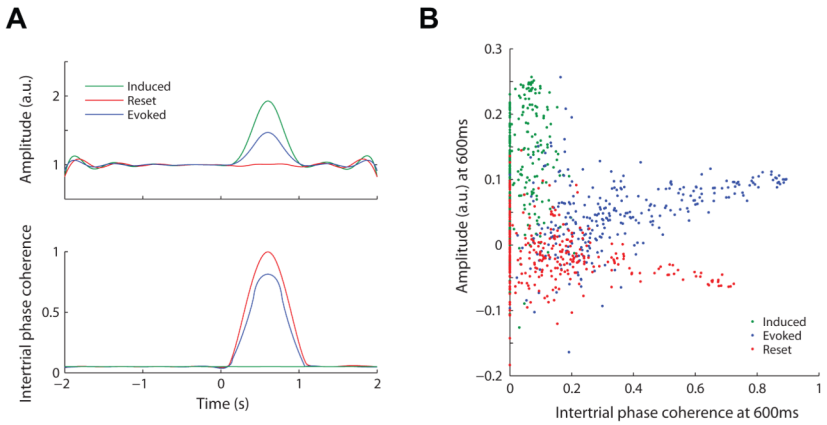

Figure 7.

Identification of underlying mechanisms in the mathematical model. **(A)** By combining amplitude information and the IPC, it is possible to distinguish between the three simulated mechanisms (Fig 2). Here, the amplitude of each trial was defined as the magnitude of the wavelet coefficient at 2Hz, and the average was taken over all 1000 trials of simulated LFP. Induced oscillations (green and Fig 2B, *left*) will produce an increase in mean amplitude after the stimulus onset (top panel) but no increase in IPC (bottom panel). An evoked potential (blue and Fig 2B, *middle*) will lead to an increase in mean amplitude concurrent with an increase in IPC. A phase reset (red and Fig 2B, *right*) will cause an increase in IPC but no increase in mean amplitude across trials. **(B)** Over all simulated electrodes, a plot of the IPC and mean amplitude at the peak of the response (600ms) results in a unique distribution of points for each mechanism. Here each point represents data from one electrode, and all three mechanisms were simulated for each electrode. The simulated signals were the same as in (A), but a varying amount of 1/f noise was added to each electrode to mimic the variability of the human LFP data. The amplitude has been rescaled by a subtraction of the pre-stimulus activity (see Methods). Note that amplitude and IPC are positively correlated in the case of the evoked potential (blue) but are uncorrelated when measured for the phase reset (red).

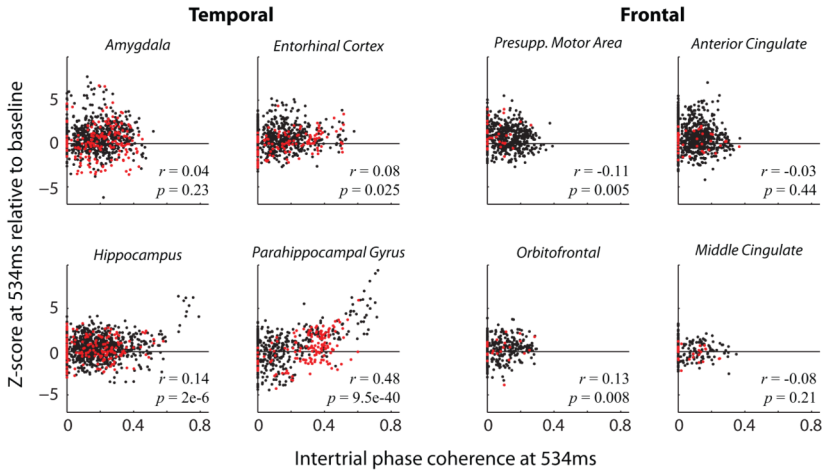

Figure 8.

Identification of underlying mechanisms in the human LFP data. As in the simulated data (Fig 7), the relationship between amplitude and IPC can provide evidence for which mechanism generated the neural response. Separated by brain region, these panels show the amplitude (as a z-score) and IPC for each bipolar measurement 534ms after the second card was revealed. This time was chosen because it is the mean of the peak IPC times for correct and incorrect trials (Fig 5). The panels show *all* bipolar measurements (black), and those associated with significant *d'* values are plotted in red. The correlation coefficient (*r*) and statistical significance (*p*) are shown in the lower right corner. The amplitude has been rescaled using a measure of the pre-stimulus activitiy (see Methods). Note that in the parahippocampal gyrus, the positive correlation between IPC and z-score is suggestive of an evoked potential. However, in the amygdala, the relatively high values of IPC and lack of positive correlation in the data matches the characteristics of phase resetting. Data from the entorhinal cortex and hippocampus are more difficult to interpret because the correlations are statistically significant but have smaller values of *r*. In the frontal lobe, the values of IPC are too low to discern which mechanism caused the neural response. This is consistent with the Rayleigh test of uniformity which indicated that the phase distributions over trials were uniform (Fig 6A,B). See also Figure S4.

Table 1

Data collected from six human subjects, along with the corresponding classification results at 2.14Hz (Fig 4) and correlation coefficients comparing amplitude and IPC (Fig 8). Five regions were measured in only one patient and are not included in this table: superior temporal gyrus, posterior temporal, fusiform gyrus, supplementary motor area, and frontal. The total number of bipolar measurements was 1,652.

Region	Data	Classification statistics		IPC/Amplitude Correlation	
		# Significant	Mean of sig. d'	1st Click	2nd Click
Temporal Lobe Regions	6 patients, 1008 bipolar measurements	162 (16.1%)	0.622	---	---
Amygdala	4 patients, 224 bipolar measurements	43 (19.2%)	0.644	R = -0.09 (p = 0.008)	R = 0.04 (N.S.)
Entorhinal Cortex	4 patients, 196 bipolar measurements	29 (14.8%)	0.715	R = 0.27 (p = 1.2e-14)	R = 0.08 (p = 0.025)
Hippocampus	6 patients, 280 bipolar measurements	39 (13.9%)	0.588	R = 0.29 (p = 9e-23)	R = 0.14 (p = 2e-6)
Parahippo-campal Gyrus	3 patients, 168 bipolar measurements	37 (22.0%)	0.701	R = 0.37 (p = 8.4e-24)	R = 0.48 (p = 9.5e-40)
Frontal Lobe Regions	6 patients, 644 bipolar measurements	36 (5.6%)	0.330	---	---
Presupp. Motor Area	3 patients, 168 bipolar measurements	8 (4.8%)	0.362	R = -0.005 (N.S.)	R = -0.11 (p = 0.005)
Anterior Cingulate	4 patients, 224 bipolar measurements	11 (4.9%)	0.300	R = 0.074 (p = 0.027)	R = -0.026 (N.S.)
Middle Cingulate	2 patients, 56 bipolar measurements	8 (14.3%)	0.352	R = 0.31 (p = 3.2e-6)	R = -0.083 (N.S.)
Orbitofrontal	2 patients, 112 bipolar measurements	6 (5.4%)	0.305	R = -0.22 (p = 3.7e-6)	R = 0.13 (p = 0.008)